Title
α2δ-3 Is Required for Rapid Transsynaptic Homeostatic Signaling

Journal
Cell Reports, 16(11)

ISSN
2639-1856

Authors
Wang, Tingting
Jones, Ryan T
Whippen, Jenna M
et al.

Publication Date
2016-09-01

DOI
10.1016/j.celrep.2016.08.030

Peer reviewed

HHS Public Access

Author manuscript

Cell Rep. Author manuscript; available in PMC 2017 September 14.

Published in final edited form as:

Cell Rep. 2016 September 13; 16(11): 2875–2888. doi:10.1016/j.celrep.2016.08.030.

α2δ-3 is Required for Rapid Trans-Synaptic Homeostatic Signaling

Tingting Wang, **Ryan T. Jones**, **Jenna M. Whippen**, and **Graeme W. Davis***

Department of Biochemistry and Biophysics, University of California San Francisco, San Francisco, CA 94158, USA

Abstract

The homeostatic modulation of neurotransmitter release, termed presynaptic homeostatic potentiation (PHP), is a fundamental type of neuromodulation, conserved from *Drosophila* to human, that stabilizes information transfer at synaptic connections throughout the nervous system. Here we demonstrate that *α2δ-3*, an auxiliary subunit of the presynaptic calcium channel, is required for PHP. The *α2δ* gene family has been linked to chronic pain, epilepsy, autism and the action of two psychiatric drugs, gabapentin and pregabalin. We demonstrate that loss of *α2δ-3* blocks both the rapid induction and sustained expression of PHP due to a failure to potentiate presynaptic calcium influx and the RIM-dependent readily-releasable vesicle pool. These deficits are independent of α2δ-3-mediated regulation of baseline calcium influx and presynaptic action potential waveform. α2δ proteins reside at the extracellular face of presynaptic release sites throughout the nervous system, an ideal site to mediate rapid, trans-synaptic homeostatic signaling in health and disease.

Graphical Abstract

*Correspondence: graeme.davis@ucsf.edu.

SUPPLEMENTAL INFORMATION

Supplemental information includes Supplemental Experimental Procedures, seven figures and one table.

AUTHOR CONTRIBUTION

Tingting Wang was responsible for the electrophysiological analysis of synaptic homeostasis in all figures as well as calcium imaging, inclusive of data analysis and figure generation and was involved in all stages of manuscript preparation. RT Jones collected and analyzed data in Figure 2 for calcium channel physiology. JM Whippen collected and analyzed data for Arch imaging. Graeme Davis is the corresponding author who contributed to experimental design, analysis and manuscript preparation.

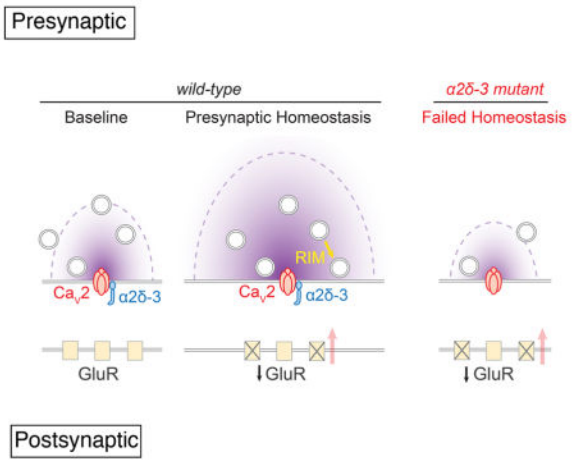

Keywords

α2δ-3; Calcium channel; $Ca_V2.1$; Presynaptic calcium influx; Readily-releasable vesicle pool; Homeostatic plasticity; Synaptic homeostasis; Synaptic transmission; Neuromuscular junction; Epilepsy; Autism; Neuropathic pain; Schizophrenia

INTRODUCTION

Presynaptic homeostatic potentiation (PHP) can be initiated by disruption of postsynaptic neurotransmitter receptors and is expressed as a change in presynaptic vesicle release (Davis, 2006, 2013; Davis and Muller, 2015). As such, PHP requires retrograde, trans-synaptic signaling (Davis, 2013; Davis et al., 1998; Petersen et al., 1997). The homeostatic potentiation of presynaptic release is mediated by increased presynaptic calcium influx (Muller and Davis, 2012) and potentiation of the readily-releasable synaptic vesicle pool (Muller et al., 2012; Weyhersmuller et al., 2011) without a change in the presynaptic action potential waveform (Gavino et al., 2015). A remarkable property of presynaptic homeostatic plasticity is that it can be induced in a time frame of seconds to minutes (Frank et al., 2006; Wang et al., 2014) and can be stably maintained throughout the life of an organism; months in *Drosophila* (Mahoney et al., 2014) and decades in human (Cull-Candy et al., 1980). Equally remarkable, presynaptic homeostasis can precisely offset the magnitude of postsynaptic perturbations that vary widely in severity (Frank et al., 2006). This implies the existence of profoundly stable and remarkably precise homeostatic modifications to the presynaptic release apparatus. Trans-synaptic signaling systems that are capable of achieving the rapid, accurate and persistent control of presynaptic vesicle release are generally unknown.

In a large-scale forward genetic screen for homeostatic plasticity genes, we identified mutations in the α2δ-3 auxiliary subunit of the $Ca_V2.1$ calcium channel (Dickman and Davis, 2009). *α2δ* genes encode a family of proteins that are post-translationally processed into a large glycosylated extracellular α2 domain that is linked through disulfide bonding to a short, membrane associated, *δ* domain (Dolphin, 2012). Existing loss of function data are consistent with the primary function of *α2δ* being the trafficking and synaptic stabilization

of pore-forming α1 calcium channel subunits, with which they associate in the endoplasmic reticulum (Bauer et al., 2010). There is also evidence that α2δ subunits control calcium channel kinetics in a channel-type and cell-type specific manner (Fuller-Bicer et al., 2009; Patel et al., 2013). However, the function of the *α2δ* gene family extends beyond calcium channel trafficking and membrane stabilization including activities related to synapse formation and stability (Christopherson et al., 2005; Eroglu et al., 2009; Kurshan et al., 2009). As such, the large, glycosylated extracellular domain in α2δ may have additional, potent signaling activities at the active zone.

Importantly, the *α2δ* gene family is associated with a wide range of neurological diseases including autism spectrum disorders (ASD, (De Rubeis et al., 2014)), neuropathic pain (D'Arco et al., 2015; Neely et al., 2010), and epilepsy (Barclay et al., 2001). The α2δ-1 and α2δ-2 proteins are the primary targets of gabapentin and pregabalin, two major drugs to treat neuropathic pain and epilepsy (Hendrich et al., 2008). Here we demonstrate that *α2δ-3* is essential for PHP. Thus, while α2δ-3 is an extracellular component of the extended presynaptic calcium channel complex (Davies et al., 2010; Gurnett et al., 1997), it none-the-less has a profound ability to modulate the intracellular neurotransmitter release mechanism. We propose that α2δ-3 relays signaling information from the synaptic cleft to the cytoplasmic face of the presynaptic active zone during PHP, an activity that could reasonably be related to the function of α2δ-3 during neurological disease.

RESULTS

α2δ-3 is Required for the Rapid Induction of Synaptic Homeostasis

Presynaptic homeostatic plasticity can be rapidly induced by application of sub-blocking concentrations of the glutamate receptor antagonist Philanthotoxin (PhTX). In wild-type animals, application of PhTX causes a ~50% decrease in the amplitude of spontaneous miniature excitatory postsynaptic potential amplitudes (mEPSP). In response to this postsynaptic perturbation, there is a homeostatic increase in presynaptic neurotransmitter release that precisely offsets the magnitude of the decrease in mEPSP amplitude. As a consequence, excitatory postsynaptic potential amplitudes (EPSP) are restored to baseline levels (Frank et al., 2006). The response to acute application of PhTX is rapid, occurring in seconds to minutes, occurs locally at the isolated NMJ and is independent of new protein translation (Frank et al., 2006). This assay was used to screen for mutations that block presynaptic homeostatic plasticity. A previously characterized mutation in the *α2δ-3* gene was screened and found to potentially disrupt the rapid induction of presynaptic homeostasis, but there were also defects in baseline neurotransmission that complicated any simple conclusion (Dickman and Davis, 2009).

To determine whether *α2δ-3* is necessary for presynaptic homeostasis we examined several, previously characterized, *α2δ-3* loss of function mutants (Dickman et al., 2008; Ly et al., 2008). Mutations in *α2δ-3* have been published as either *α2δ-3* or *straightjacket* (*stj*) depending on how they were initially isolated and we have retained this nomenclature. The published *α2δ-3* alleles that we use include: $\alpha2\delta\text{-}3^{106}$ (null mutation, www.flybase.org), $\alpha2\delta\text{-}3^{k10814}$ (transposon insertion *p[lacW]stj[k10814]*, hypomorphic mutation), stj^{1} (strong loss-of-function mutation), stj^{2} (strong loss-of-function mutation) and a deficiency mutation

that uncovers the entire *α2δ-3* gene (*$Df^{(2R)Exel7128}$*; see Figure 1A for annotation to the *α2δ-3* gene locus). The homozygous *$α2δ\text{-}3^{106}$* mutation causes lethality at the late-embryonic stage (Dickman et al., 2008; Kurshan et al., 2009). As a consequence, we performed most of our studies using flies harboring trans-allelic combinations that survive to the third instar stage.

When we assay the rapid induction of PHP, we find that application of PhTX caused a significant reduction of mEPSP amplitude in all genotypes (Figure 1B, 1C and Figure S1, S2). At the wild-type (wt) and heterozygous *α2δ-3* mutant synapses (*$α2δ\text{-}3^{k10814}/+$*, *$α2δ\text{-}3^{106}/+$* and *$Df^{(2R)Exel7128}/+$*) an increase in presynaptic release offsets the change in mEPSP amplitude and restores EPSP amplitudes to normal baseline level (Figure 1B, 1C and Figure S1, S2). However, the homeostatic change in presynaptic release was blocked in every loss of function allelic combination of *α2δ-3* mutations that we analyzed (Figure 1B, 1C and Figure S1, S2). Presynaptic release is defined as quantal content (quantal content = EPSP/mEPSP; see methods). From these data, we conclude that loss-of-function mutations in *α2δ-3* prevent the rapid induction of PHP. Sample sizes for all figures are reported in Figure Legends and Supplemental Table S1.

We considered the possibility that impaired presynaptic homeostasis is caused by loss of the α1 subunit encoded by the *cacophony* (*cac*) gene. However, several observations argue against this idea. First, we note that presynaptic homeostasis is blocked regardless of the severity of the *α2δ-3* allelic combination tested. EPSP amplitudes are decreased by ~30% in *$α2δ\text{-}3^{k10814}/α2δ\text{-}3^{106}$* and by ~50% in *$stj^{1}/stj^{2}$* (Figure S2), but homeostatic plasticity is completely blocked in both instances (Figure 1 and S2). Second, although missense mutations in the *cac* gene have been shown to block presynaptic homeostasis (Frank et al., 2009), RNAi-mediated depletion of the α1 subunit from the presynaptic terminal, sufficient to cause an ~80% reduction in EPSP amplitude compared to controls, did not impair presynaptic homeostasis (Brusich et al., 2015). An independent study made a similar observation, showing that reduced $Ca_V2.1$ channel abundance and a correlated ~50% decrease in single action potential (AP) induced calcium influx, did not impair the rapid induction of presynaptic homeostasis (Gavino et al., 2015). Third, synaptic homeostasis is fully expressed over a 50-fold range of extracelluar calcium concentration (0.3 to 15mM $[Ca^{2+}]_e$) (Muller et al., 2015), arguing that the absolute amount of calcium influx per action potential does not influence the homeostatic modulation of presynaptic neurotransmitter release. Here, we confirm this finding in the *α2δ-3* mutant background. We recorded from *stj* alleles at an elevated extracellular calcium concentration (1mM $[Ca^{2+}]_e$) that restores EPSP amplitudes to values observed in wild-type when recorded in 0.3mM $[Ca^{2+}]_e$. Homeostatic plasticity remains completely blocked (Figure S2). Collectively, these data argue that the abundance of the $Ca_V2.1$ α1 subunit and the absolute amount of presynaptic calcium influx per action potential does not influence the homeostatic modulation of synaptic transmission. By extension, these data argue that *α2δ-3* has an activity that is necessary for presynaptic homeostasis, which is independent of the control of α1 subunit abundance or total presynaptic calcium influx.

Presynaptic Expression of *α2δ-3* Restores Synaptic Homeostasis in *α2δ-3.*

We have performed tissue-specific genetic rescue experiments to demonstrate that the observed block of synaptic homeostasis is specifically caused by the loss of *α2δ-3*. We expressed *α2δ-3* under UAS control (*UAS-stj*), with and without an epitope tag (*UAS-stj-3HA*). We did so tissue-specifically in either neurons (*elav^{C155}-Gal4*) or muscle (*MHC-Gal4*) in the *α2δ-3* mutant background. Neuronal expression of *UAS-stj* restores all aspects of baseline transmission to wild-type levels (Figure S3). By contrast, postsynaptic expression of *UAS-stj* fails to rescue EPSP amplitude and quantal content (Figure S3). We then show that neuronal expression of *UAS-stj* rescues PHP in the *α2δ-3* mutant, whereas muscle-specific expression does not (Figure 1D and 1E). Thus, presynaptic *α2δ-3* is required for the rapid induction of PHP.

α2δ-3 is Necessary for the Sustained Expression of Synaptic Homeostasis

Presynaptic homeostasis can also be induced by genetic deletion of the muscle-specific glutamate receptor subunit *GluRIIA* (Petersen et al., 1997). This not only provides a second method to assay the induction of presynaptic homeostasis, it is also a muscle-specific perturbation that is present throughout larval life. As such, analysis of *GluRIIA* mutants has been used to assay the persistent expression of presynaptic homeostasis. Here, we demonstrate that presynaptic homeostasis is blocked in the *GluRIIA^{sp16}*, *α2δ-3* double mutants (Figure 1F–1I). Specifically, there is a large decrease in mEPSP amplitude caused by the *GluRIIA^{sp16}* mutation compared to wild-type and this is correlated with a large increase in presynaptic release (quantal content) that brings EPSP amplitudes back toward wild-type value (Figure 1H and 1I). In the *GluRIIA^{sp16}*, *α2δ-3* double mutants there is an even larger percent decrease in EPSP amplitude compared to *α2δ-3* mutant alone, but there is no corresponding increase in presynaptic release, demonstrating that the sustained expression of PHP requires *α2δ-3* (Figure 1H and 1I).

α2δ-3 Mutants with Impaired Presynaptic Homeostasis Exhibit Normal Active Zone Number

It has been reported previously that loss of *α2δ-3* can influence the anatomical growth of the *Drosophila* NMJ (Dickman et al., 2008; Kurshan et al., 2009). We revisited this analysis to determine if a change in active zone number or organization might contribute to the defects in presynaptic homeostasis that we observe in the loss-of-function alleles examined here. We find that total active zone number, determined by quantification of Brp-labeled presynaptic active zones, is not changed in *α2δ-3* mutants (anti-Brp, Figure S4A and S4B; (Kittel et al., 2006)). We also observe a reduction of total postsynaptic area (assessed by quantification of Dlg staining) and total bouton number in *α2δ-3* compared to wild-type (Figure S4C and S4D). As a consequence each synaptic bouton encompasses an increased number of active zones (Figure S4F). Synapse morphology remains unchanged in *α2δ-3* compared to wild-type at muscle 4 (Figure S5). From these data, we conclude that impaired presynaptic homeostasis in the mutants that we have analyzed is not a secondary consequence of decreased active zone number.

α2δ-3 Mutations Have Reduced Calcium Current Density and Decreased Presynaptic Calcium Influx

Somatic recordings and calcium current isolations were achieved according to standard protocols (see methods). We find that the hypomorphic *α2δ-3* mutant (*α2δ-3*^{106}/*α2δ-3*^{k10814}) has a significant decrease in the peak calcium current (Figure 2A and 2B) without a change in voltage-dependent activation and steady-state inactivation (Figure 2C). The calcium currents activate at approximately -20mV, consistent with these currents being high-voltage activated $Ca_V2.1$ currents. The peak calcium currents reverse at approximately +50mV, as expected for $Ca_V2.1$ channels. Finally, RNAseq analysis of isolated motoneurons confirms that $Ca_V2.1$ is the only highly expressed calcium channel in these neurons (RJ, JW and GWD, unpublished data). Based on these data, we conclude that loss of *α2δ-3* causes a significant reduction in the $Ca_V2.1$ calcium current density, without altering the voltage dependence of channel activation or inactivation.

We next measured single action potential induced calcium influx at presynaptic boutons in wild-type and the *α2δ-3*^{106}/*α2δ-3*^{k10814} mutant according to published methods (Muller and Davis, 2012; Muller et al., 2015; Wang et al., 2014; Younger et al., 2013). Presynaptic calcium influx is significantly decreased by ~40% in the *α2δ-3*^{106}/*α2δ-3*^{k10814} mutant (Figure 2E and 2F). There was no significant change in either baseline OGB-1 fluorescence or the time constant of calcium signal decay (Figure 6D and 6E), indicating equivalent dye loading across genotypes and a similar capacity for calcium buffering/extrusion in the *α2δ-3*^{106}/*α2δ-3*^{k10814}mutant. There is remarkable concordance between the decrease in somatically recorded calcium currents and presynaptic AP-triggered calcium influx in the *α2δ-3*^{106}/*α2δ-3*^{k10814} mutant (Figure 2B and 2E). However, since active zone number per synaptic bouton is increased in the *α2δ-3* mutant compared to wild-type, calcium influx per active zone is likely to be decreased to a greater extent than revealed by the spatially averaged calcium transient. Although we cannot rule out an action of *α2δ-3* mutants on calcium current kinetics at the presynaptic terminal, our data strongly suggest that the primary effect of the *α2δ-3*^{106}/*α2δ-3*^{k10814}mutant is to reduce calcium current density. However, since reduced calcium influx alone does not disrupt presynaptic homeostatic plasticity (see above; (Brusich et al., 2015; Gavino et al., 2015)), there must be additional activities of *α2δ-3*, in addition to its role in controlling $Ca_V2.1$ channel abundance, that are necessary for PHP.

Presynaptic Action Potential Waveforms Assessed with Archaerhodopsin Voltage Imaging

Recent work in cultured hippocampal neurons has shown that RNAi-mediated knockdown of *α2δ-1* causes a ~30% increase in action potential (AP) width at half-max (Hoppa et al., 2014), an effect that the authors link, pharmacologically, to a change in presynaptic potassium channel activity (Hoppa et al., 2014). We recently demonstrated that presynaptic homeostatic potentiation and depression can be invoked without a change in presynaptic AP waveform (Ford and Davis, 2014; Gavino et al., 2015). None-the-less, changes in AP waveform, indicative of changes in the presynaptic membrane excitability, could conceivably alter the expression of PHP.

We recently adopted the use of transgenically encoded, voltage-sensitive Archaerhodopsin (Hoppa et al., 2014; Kralj et al., 2012) to image action potential waveforms at the *Drosophila* NMJ (Ford and Davis, 2014; Gavino et al., 2015). Expression of *UAS-Archaerhodopsin-GFP* (*UAS-Arch*; Figure 3A) in motoneurons has no effect on presynaptic homeostasis or baseline neurotransmitter release (Ford and Davis, 2014; Gavino et al., 2015). Expression of *UAS-Arch* also has no effect on baseline neurotransmission in wild-type or in the *α2δ-3* mutants (Figure S6). However, when we examine the action potential waveform in *α2δ-3* mutants, we find that AP repolarization is significantly accelerated compared to wild-type, revealed as a significant decrease in width at half-maximal amplitude (width half-max) (Figure 3B and 3C; see methods and (Ford and Davis, 2014; Gavino et al., 2015)). This effect is not caused by diminished presynaptic calcium influx in the *α2δ-3* mutants. To show this, we measured AP waveform and amplitude prior to and following application of Cd^{2+} (3μM) to block calcium influx (Frank et al., 2006). We find no change in AP amplitude in the presence of Cd^{2+} (Figure 3D). In addition, action potential repolarization is slowed, rather than accelerated, in the presence of Cd^{2+} (3μM) or the absence of external calcium (Ford and Davis, 2014). Thus, the acceleration of AP repolarization must be caused by other mechanisms, possibly a change in potassium channel expression or activity, as suggested by work in mammalian neurons examining *α2δ-1* (Hoppa et al., 2014).

Next, we sought to determine whether accelerated AP repolarization in *α2δ-3* occludes presynaptic homeostasis. First, we repeated measurements of AP repolarization in wild-type and *α2δ-3* at 0.3mM extracellular calcium and observe a similar acceleration of AP repolarization in the *α2δ-3* mutant (Figure 3E and 3F). Next, we determined a concentration of 4-aminopyridine (4-AP; 100μM) that would slow AP repolarization in *α2δ-3* to the same rate observed in wild-type in the absence of 4-AP (Figure 3E–J). Then, we asked whether application of 100μM 4-AP would rescue presynaptic homeostasis in *α2δ-3*, also assessed at 0.3mM extracelluar calcium. It does not. 4-AP treatment does not change EPSP amplitude or quantal content in *α2δ-3* recorded in the presence of PhTX to induce PHP (Figure 3K–3M). Thus, acceleration of AP repolarization in *α2δ-3* does not cause the observed block in presynaptic homeostasis. The underlying cause of accelerated AP repolarization in *α2δ-3* remains unclear and will be a topic of future investigation, independent of the analysis of synaptic homeostasis.

α2δ-3 is Necessary for the Homeostatic Modulation of Presynaptic Calcium Influx

We previously demonstrated that the expression of presynaptic homeostasis is mediated, in part, by the homeostatic potentiation of presynaptic calcium influx (Muller and Davis, 2012). Therefore, we sought to determine whether *α2δ-3* mutants block this process. As shown above, the average peak amplitude of single AP-evoked calcium transients in the *α2δ-3* mutants is significantly reduced compared to wild-type (Figure 4A–4C). We then confirmed that calcium influx is potentiated at wild-type synapses in the presence of PhTX, compared to non-treated synapses (Figure 4A–4C). Finally, we assayed the *α2δ-3* mutant and find that there is no PhTX-dependent increase of calcium influx (Figure 4A–4C). Importantly, baseline OGB-1 fluorescence was statistically unchanged comparing boutons in the presence or absence of PhTX in both wild-type and the *α2δ-3* mutant (Figure 4D). Thus,

the homeostatic modulation of presynaptic calcium influx is blocked at the *α2δ-3* mutant NMJ. We note that there is a significant decrease in the time constant of calcium transient decay at wild-type synapses in the presence of PhTX (Figure 4E; see also (Muller and Davis, 2012)). By contrast, no such change in calcium transient decay kinetics was observed at the *α2δ-3* mutant synapses in the presence of PhTX (Figure 4E). These data further support a function for *α2δ-3* in the homeostatic control of presynaptic calcium influx. The cause of the PhTX-dependent acceleration of calcium signal decay remains unknown.

α2δ-3 Regulates RRP Size during Presynaptic Homeostasis

The mechanisms of presynaptic homeostasis also require an increase in the size of the readily-releasable vesicle pool (RRP) (Muller et al., 2012; Weyhersmuller et al., 2011). The inter-cellular signaling mechanisms that determine the homeostatic expansion of the RRP remain largely unknown (Harris et al., 2015). Here, we estimate RRP size by measuring cumulative EPSC amplitude during a high frequency stimulus train (60Hz, 30 stimuli; (Schneggenburger et al., 1999; Thanawala and Regehr, 2013)) at elevated extracellular calcium (1.5mM; Figure 5). First, we observe a dramatic reduction of the cumulative EPSC amplitude in *α2δ-3* compared to wild-type (Figure 5A, 5B and 5E) demonstrating a significant reduction of the baseline RRP in *α2δ-3*. Next, we verify a homeostatic increase of the apparent RRP in wild-type caused by application of PhTX (Figure 5C, F). Then, we demonstrate that the initial EPSC amplitude and the cumulative EPSC amplitude are both significantly reduced in the presence of PhTX in *α2δ-3* (Figure 5D and 5E). When we calculate the apparent RRP, we find that the homeostatic expansion of the apparent RRP is blocked in *α2δ-3* (Figure 5F). Thus, *α2δ-3* is essential for the homeostatic expansion of the RRP (see discussion).

The disruption of baseline RRP in *α2δ-3* is quite remarkable given that previous studies have shown that there is no change in the number of active-zone localized synaptic vesicles in *α2δ-3* mutants (Ly et al., 2008). If the change in RRP was solely due to decreased presynaptic calcium influx, we might expect to observe facilitation during a stimulus train. Indeed, EPSCs depress more slowly in *α2δ-3* compared to wild-type (Figure 5G–5I). However, the decrease in synaptic depression in *α2δ-3* is quite modest given the large decrease in calcium influx that we have quantified (Figure 2). To further examine this issue, we normalize the first EPSC amplitude of wild-type to levels observed in the *α2δ-3* mutant by reducing external calcium to 0.6mM in wild-type. When we make this comparison (wild-type at 0.6mM $[Ca^{2+}]_e$ compared to *α2δ-3* mutant at 1.5mM $[Ca^{2+}]_e$), the initial EPSCs are equivalent but the wild-type synapse facilitates while the *α2δ-3* synapse depresses (Figure 5J and 5K). Thus, loss of *α2δ-3* appears to have an effect on vesicle release that is more severe than can be accounted for by the decrease ininitial calcium influx. Since vesicle number and distribution are unaltered in *α2δ-3* (Ly et al., 2008), these data suggest that loss of *α2δ-3* controls the availability of vesicles that reside at the active zone for synaptic transmission. As such, the large decrease in the RRP in *α2δ-3* compared to wild-type is caused by the combined effect of decreased calcium entry and a decreased number of fusion competent vesicles (see discussion).

α2δ-3 Mutants Exhibit Increased EGTA Sensitivity

Prior work at cultured hippocampal synapses demonstrates that overexpression of *α2δ-1* causes synaptic transmission to become less sensitive to the effects of the calcium buffer EGTA-AM (Hoppa et al., 2012). EGTA has a relatively slow calcium binding rate (Smith et al., 1984) and has been used to probe the functional coupling of vesicle to sites of presynaptic calcium influx (Schneggenburger and Neher, 2005). Here, we tested the effects of EGTA-AM (25μM) on single AP-evoked EPSC amplitudes (1.5mM $[Ca^{2+}]_e$) at wild-type and *α2δ-3* mutant synapses (Figure 6). EGTA-AM has no effect on the wild-type synapse (Figure 6A). However, EGTA-AM causes a significant decrease in EPSC amplitude at the *α2δ-3* synapses (Figure 6A, 6C and 6D). Next, we lowered extracellular calcium in wild-type (0.6mM $[Ca^{2+}]_e$), again normalizing initial release to that observed in *α2δ-3* at 1.5mM $[Ca^{2+}]_e$. Regardless, EGTA-AM still has a significantly greater effect in *α2δ-3* compared to wild-type (Figure 6C-6E). These data suggest that loss of *α2δ-3* impairs the coupling of vesicles to presynaptic calcium channels, consistent with prior observations in mammalian cell culture (Hoppa et al., 2012).

α2δ-3 Genetically Interacts with RIM for the Expression of Synaptic Homeostasis

The pore-forming α1 subunit of presynaptic calcium channels interacts with Rab3 Interacting Molecule (RIM) and Rim-Binding Protein (RBP) (Sudhof, 2012). Both RIM and RBP are necessary for presynaptic homeostasis, and mutations in both genes show increased EGTA sensitivity compared to wild-type (Muller et al., 2015; Muller et al., 2012). Therefore, we speculate that signaling might be relayed from α2δ-3 to RIM or RBP at baseline and during presynaptic homeostasis. To explore this possibility, we examined whether *α2δ-3* genetically interacts with *rim*. Heterozygous mutations in either *rim* ($rim^{103}/+$) or *α2δ-3* ($\alpha2\delta\text{-}3^{106}/+$) have no effect on baseline neurotransmitter release or presynaptic homeostasis (Figure 7B–7E). When we examine the double heterozygous animals ($\alpha2\delta\text{-}3^{106}/+;rim^{103}/+$) we find that baseline presynaptic release is unaltered compared to wild-type (Figure 7E). There is a small decrease in EPSC amplitude in the double heterozygous condition (Figure 7D), but this decrease is caused by a decrease in mEPSP amplitude (Figure 7C) without a change in quantal content (Figure 7E). However, presynaptic homeostasisis completely blocked in the double heterozygous animals (Figure 7B, 7D and 7E). This genetic interaction between *α2δ-3* and *rim* was also confirmed at low extracellular calcium (Figure S7). The demonstration that presynaptic homeostasis is blocked in the absence of an effect on baseline release argues strongly that *α2δ-3* has a signaling role during homeostatic plasticity that is independent of its function to control calcium channel abundance. This function could be mediated through RIM, though additional evidence is necessary to make such a conclusion.

We then tested for a genetic interaction with *rim-binding protein* (*drbp*). Again, we find that the heterozygous $drbp^{stop1}/+$ mutation (a molecular null mutation) has no effect on baseline neurotransmitter release or presynaptic homeostasis (Figure 7C–E). When we examine the double heterozygous mutant combination of $drbp^{stop1}/+$ and $\alpha2\delta\text{-}3^{106}/+$, we find a significant decrease in baseline release (Figure 7C–E). Remarkably, however, we observe robust expression of presynaptic homeostasis in the double heterozygous mutant (Figure 7B and 7E). The magnitude of homeostatic compensation in this double heterozygous mutant is

not significantly different than either wild-type or the heterozygous mutations alone (Figure 7B; p>0.05, one-way ANOVA, Bonferroni's test). These data argue for the specificity of the genetic interaction between *rim* and *α2δ-3* and support the possibility that *α2δ-3* may relay signaling from the synaptic cleft to RIM during presynaptic homeostasis.

DISCUSSION

Here we demonstrate that *α2δ-3* is essential for the rapid induction and sustained expression of presynaptic homeostatic potentiation (PHP). *α2δ-3* encodes a glycosylated extracellular protein known to interact with matrix proteins that reside within the synaptic cleft (Christopherson et al., 2005; Eroglu et al., 2009). As such, we propose that α2δ-3 mediates homeostatic, retrograde signaling by connecting signaling within synaptic cleft to effector proteins within the presynaptic terminal, such as RIM. Since α2δ-3 associates with the pore-forming α1 subunit of calcium channels, it is ideally positioned to relay signaling to the site of high-release probability vesicle fusion adjacent to the presynaptic calcium channels.

It was previously demonstrated that PHP not only requires potentiation of presynaptic calcium influx, but also requires a parallel homeostatic expansion of the RRP (Harris et al., 2015; Muller et al., 2015; Muller et al., 2012; Weyhersmuller et al., 2011). Several lines of evidence argue against the possibility that the homeostatic potentiation of presynaptic calcium influx fully accounts for the observed potentiation of the RRP. First, it is well-established in mammalian systems (Thanawala and Regehr, 2013) and the *Drosophila* NMJ (Muller et al., 2015) that the calcium-dependence of the RRP is sub-linear. Therefore, the relatively small change in presynaptic calcium influx that occurs during PHP (12–25%) would not be sufficient to account for the observed doubling of the RRP, an effect that has been quantified across a wide range of extracellular calcium (0.3–15mM $[Ca^{2+}]_e$) (Muller et al., 2015). Second, the homeostatic increase of presynaptic calcium influx and the homeostatic expansion of RRP are genetically separable processes (Harris et al., 2015; Muller et al., 2012). Since loss of *α2δ-3* completely blocks the homeostatic expansion of the RRP, it appears that α2δ-3 has an additional activity that is directed at the homeostatic modulation of the RRP.

Collectively, our data argue that *α2δ-3* functions with *rim*, either directly or indirectly, to achieve a homeostatic potentiation of the RRP. First, the loss of function phenotype of *α2δ-3* is strikingly similar to that observed in *rim* mutants. Both mutations cause a deficit in presynaptic release that is associated with diminished baseline presynaptic calcium influx, diminished size of the baseline RRP and enhanced sensitivity to application of EGTA-AM (Muller et al., 2012). Second, we demonstrate a strong trans-heterozygous interaction between *rim/+* and *α2δ-3/+*, suggesting that both genes function to control the same presynaptic processes during PHP. Since the *rim* mutation selectively disrupts the homeostatic modulation of the RRP it suggests that this genetic interaction reflects a failure to homeostatically modulate the RRP.

Both RIM and α2δ-3 bind the pore forming α1 subunit of the $Ca_V2.1$ calcium channel. As such, signaling could be relayed from α2δ-3 to RIM through molecular interactions within the extended $Ca_V2.1$ calcium channel complex. However, not all evidence is consistent with

this possibility. For example, RNAi-mediated depletion of $Ca_V2.1$ channels, sufficient to decrease release by ~80% does not prevent presynaptic homeostasis (Brusich et al., 2015). Thus, loss of α2δ-3 blocks PHP whereas loss of $Ca_V2.1$ α1 subunit does not. In addition, the double heterozygous mutant of *rim/+* and *α2δ-3/+* blocks PHP, but does not disrupt baseline vesicle release, arguing that this genetic interaction is not due to a decrease in the number or organization of presynaptic α1 calcium channel subunits. Thus, we speculate that α2δ-3 conveys signaling through a co-receptor on the plasma membrane to participate in the homeostatic modulation of the RRP. To our knowledge, there are very few extracellular proteins known to establish baseline levels of primed, fusion competent synaptic vesicles. Since α2δ proteins should reside at chemical synapses throughout the nervous system, this signaling could reasonably be related to the neurological and psychiatric diseases associated with α2δ genes.

EXPERIMENTAL PROCEDURES

Fly Stocks and Genetics

All fly stocks were maintained at 22–25°C on normal food. The *α2δ-3*^{k10814}, *α2δ-3*^{106} and *df*$^{(2R)Exel7128}$ were generous gifts from Yuh-Nung Jan (University of California, San Francisco; Howard Hughes Medical Institute). *stj*^{1}(BL39714) and *stj*^{2}(BL39715) were obtained from Bloomington *Drosophila* Stock Center. Flies bearing *UAS-stj* (F001495) and *UAS-stj-3HA* (F001252) were obtained from FlyORF (University of Zurich). Flies harboring the *GluRIIA*^{sp16}(Petersen et al., 1997) mutation and Archaerhodopin-3 transgene *UAS-Arch* (Ford and Davis, 2014) are maintained in the Davis lab. Transgenic expression was performed using the following GAL4 drivers, *elav*^{C155}*-Gal4* (neuron-specific), *OK371-Gal4* (motoneuron-specific), and *MHC-Gal4* (muscle-specific). Unless otherwise noted, the *w*^{1118} strain was used as a wild-type (wt) control.

Electrophysiology

Sharp-electrode recordings were made from muscle 6 in abdominal segments 2 and 3 in third-instar larvae using a Multiclamp 700B amplifier (Molecular Devices). Two-electrode voltage-clamp recordings were performed using an Axoclamp 2B amplifier. HL3 saline was used (in mM): 70 NaCl, 5 KCl, 10 $MgCl_2$, 10 $NaHCO_3$, 115 Sucrose, 5 Trehalose, 5 HEPES, and 0.3 $CaCl_2$ (unless specified otherwise). EPSP and mEPSP traces were analyzed in Igor Pro (WaveMetrics) with customized routines and MiniAnalysis (Synaptosoft). For rapid induction of synaptic homeostasis, larvae were incubated in 20μM Philanthotoxin-433 in an unstretched, partially dissected preparation (PhTX, Sigma-Aldrich) for 10min (Frank et al., 2006). For EGTA experiments, unstretched, partially dissected third-instar larvae were incubated in EGTA-AM (Invitrogen) in calcium free HL3 for 10min (Muller et al., 2012). After EGTA application, the preparation was washed with calcium free HL3 (10 times) and recordings were performed in HL3 at the specified calcium concentration. For each NMJ, the average amplitude of evoked EPSP or EPSC are based on the mean peak amplitudes in response to 20–30 individual stimuli. Spontaneous mEPSPs were recorded continuously 60–90s. Quantal content was estimated for each NMJ as the ratio of EPSP or EPSC amplitude/mEPSP amplitude. The mean value across all NMJ for a given genotype is reported.

Whole-cell Patch Clamp and Calcium Current Measurement

Whole-cell patch clamp recordings were made in motorneurons (MNs) from third-instar wild-type and $\alpha2\delta\text{-}3^{k10814}/\alpha2\delta\text{-}3^{106}$ larvae. Voltage clamp recordings were made with an Axon 200B amplifier (Molecular Devices), digitized at 20kHz with a Digidata 1440A, and recorded using Clampex 10.3. Cells were held at -70mV after obtaining stable whole-cell configuration and series resistance and capacitance were compensated (> 85% predict./corr.). Whole-cell Ca^{2+} currents (I_{Ca}) were evaluated using the following protocol: from a holding potential of −70mV, a 1s prepulse to -90mV was applied, followed by a series of voltage steps (−90 to +50mV, +10mV/step, 120ms duration, 0.1Hz inter-step interval). The peak I_{Ca} currents were measured, normalized to whole-cell capacitance, and current-voltage (I-V plots) constructed by plotting verses respective voltage steps. Leak currents were subtracted offline. Ca^{2+} (1.5mM $CaCl_2$) and Ba^{2+} (1.5mM $BaCl_2$) were used as charge carriers to enhance macroscopic currents. Steady-state I_{Ca} inactivation was evaluated using the following protocol: from a holding potential of −70mV, prepulse steps (−80 to +50mV, +10mV/step, 1s duration) followed by a 6ms repolarization to the holding potential and a subsequent test depolarization to +10mV (120ms duration). I/I_{max} plots were constructed by from the normalized peak I_{Ca} and plotting it vs. the respective prepulse potential (see Supplemental Experimental Procedures for details.)

RRP Measurement

The RRP size is estimated by the method of cumulative EPSC amplitude (Muller et al., 2012; Schneggenburger et al., 1999; Weyhersmuller et al., 2011). Muscles were clamped to −65mV in two-electrode voltage configuration and EPSC amplitudes during a stimulus train at 60Hz were calculated. The average cumulative EPSC amplitude for given muscle was obtained by back-extrapolating a line fit to the linear phase (the last 200ms) of the cumulative EPSC plot to time 0. The apparent RRP size was obtained by dividing the cumulative EPSC amplitude derived from cumulative EPSC plot at time 0 by the mean mEPSP amplitude recorded in the same cell in current clamp mode before placing the second electrode in the muscle.

Immunocytochemistry

Standard immunocytochemistry was performed as previously described and see Supplemental Experimental Procedures for details (Wang et al., 2014).

Image Acquisition and Analysis

Deconvolution imaging for synapse morphology was performed using a 100x (1.4 NA) plan Apochromat objective (Carl Zeiss) on an Axiovert 200 inverted microscope (Carl Zeiss) equipped with a cooled CCD camera (CoolSNAP HQ, Roper Scientific). Image acquisition and analysis were performed in SlideBook software (Intelligent Imaging Innovation). Maximum projections of deconvolved images were used for analyses.

Calcium Imaging

Calcium imaging experiments at the third instar NMJ were performed as previously described (Muller and Davis, 2012), co-loading the motor axons with Oregon-Green 488

BAPTA-1 (OGB-1, Invitrogen) and Alexa 568 (Invitrogen). Image acquisition was performed at room temperature using a confocal laser-scanning system (Ultima, Prairie Technologies) equipped with excitation light (488 nm) from an air-cooled krypton-argon laser, 60x objective (1.0 NA, Olympus), and a gallium arsenide phosphide-based photocathode photomultiplier tube (Hamamatsu). Line scans across single boutonswere made at a frequency of 568Hz. Calciumimaging data were acquired using Prairie View (Prairie Technologies, now Bruker) and analyzed in Igor Pro (Wavemetrics).

Arch Imaging

Arch imaging and analyses were performed using confocal spot imaging according to previously published methods and see Supplemental Experimental Procedures for details (Ford and Davis, 2014).

Supplementary Material

Refer to Web version on PubMed Central for supplementary material.

Acknowledgments

We thank Özgür Genç and Nathan Harris for critical reading of the manuscript. We thank Martin Müller, Gama Ruiz and Amy Tong for technical assistance. Work in the laboratory of G.W.D. was supported by NIH grants NS059867 and NS039313. T.W. was supported by NIH NRSA postdoc fellowship NIH NINDS 1F32NS081884-02/03.

References

Barclay J, Balaguero N, Mione M, Ackerman SL, Letts VA, Brodbeck J, Canti C, Meir A, Page KM, Kusumi K, et al. Ducky mouse phenotype of epilepsy and ataxia is associated with mutations in the Cacna2d2 gene and decreased calcium channel current in cerebellar Purkinje cells. J Neurosci. 2001; 21:6095–6104. [PubMed: 11487633]

Bauer CS, Tran-Van-Minh A, Kadurin I, Dolphin AC. A new look at calcium channel alpha2delta subunits. Curr Opin Neurobiol. 2010; 20:563–571. [PubMed: 20579869]

Brusich DJ, Spring AM, Frank CA. A single-cross, RNA interference-based genetic tool for examining the long-term maintenance of homeostatic plasticity. Front Cell Neurosci. 2015; 9:107. [PubMed: 25859184]

Christopherson KS, Ullian EM, Stokes CC, Mullowney CE, Hell JW, Agah A, Lawler J, Mosher DF, Bornstein P, Barres BA. Thrombospondins are astrocyte-secreted proteins that promote CNS synaptogenesis. Cell. 2005; 120:421–433. [PubMed: 15707899]

Cull-Candy SG, Miledi R, Trautmann A, Uchitel OD. On the release of transmitter at normal, myasthenia gravis and myasthenic syndrome affected human end-plates. J Physiol. 1980; 299:621–638. [PubMed: 6103954]

D'Arco M, Margas W, Cassidy JS, Dolphin AC. The upregulation of alpha2delta-1 subunit modulates activity-dependent Ca2+ signals in sensory neurons. J Neurosci. 2015; 35:5891–5903. [PubMed: 25878262]

Davies A, Kadurin I, Alvarez-Laviada A, Douglas L, Nieto-Rostro M, Bauer CS, Pratt WS, Dolphin AC. The alpha2delta subunits of voltage-gated calcium channels form GPI-anchored proteins, a posttranslational modification essential for function. Proc Natl Acad Sci U S A. 2010; 107:1654–1659. [PubMed: 20080692]

Davis GW. Homeostatic control of neural activity: from phenomenology to molecular design. Annu Rev Neurosci. 2006; 29:307–323. [PubMed: 16776588]

Davis GW. Homeostatic signaling and the stabilization of neural function. Neuron. 2013; 80:718–728. [PubMed: 24183022]

Davis GW, DiAntonio A, Petersen SA, Goodman CS. Postsynaptic PKA controls quantal size and reveals a retrograde signal that regulates presynaptic transmitter release in Drosophila. Neuron. 1998; 20:305–315. [PubMed: 9491991]

Davis GW, Muller M. Homeostatic control of presynaptic neurotransmitter release. Annu Rev Physiol. 2015; 77:251–270. [PubMed: 25386989]

De Rubeis S, He X, Goldberg AP, Poultney CS, Samocha K, Cicek AE, Kou Y, Liu L, Fromer M, Walker S, et al. Synaptic, transcriptional and chromatin genes disrupted in autism. Nature. 2014; 515:209–215. [PubMed: 25363760]

Dickman DK, Davis GW. The schizophrenia susceptibility gene dysbindin controls synaptic homeostasis. Science. 2009; 326:1127–1130. [PubMed: 19965435]

Dickman DK, Kurshan PT, Schwarz TL. Mutations in a Drosophila alpha2delta voltage-gated calcium channel subunit reveal a crucial synaptic function. J Neurosci. 2008; 28:31–38. [PubMed: 18171920]

Dolphin AC. Calcium channel auxiliary alpha2delta and beta subunits: trafficking and one step beyond. Nat Rev Neurosci. 2012; 13:542–555. [PubMed: 22805911]

Eroglu C, Allen NJ, Susman MW, O'Rourke NA, Park CY, Ozkan E, Chakraborty C, Mulinyawe SB, Annis DS, Huberman AD, et al. Gabapentin receptor alpha2delta-1 is a neuronal thrombospondin receptor responsible for excitatory CNS synaptogenesis. Cell. 2009; 139:380–392. [PubMed: 19818485]

Ford KJ, Davis GW. Archaerhodopsin voltage imaging: synaptic calcium and BK channels stabilize action potential repolarization at the Drosophila neuromuscular junction. J Neurosci. 2014; 34:14517–14525. [PubMed: 25355206]

Frank CA, Kennedy MJ, Goold CP, Marek KW, Davis GW. Mechanisms underlying the rapid induction and sustained expression of synaptic homeostasis. Neuron. 2006; 52:663–677. [PubMed: 17114050]

Frank CA, Pielage J, Davis GW. A presynaptic homeostatic signaling system composed of the Eph receptor, ephexin, Cdc42, and CaV2.1 calcium channels. Neuron. 2009; 61:556–569. [PubMed: 19249276]

Fuller-Bicer GA, Varadi G, Koch SE, Ishii M, Bodi I, Kadeer N, Muth JN, Mikala G, Petrashevskaya NN, Jordan MA, et al. Targeted disruption of the voltage-dependent calcium channel alpha2/delta-1-subunit. Am J Physiol Heart Circ Physiol. 2009; 297:H117–124. [PubMed: 19429829]

Gavino MA, Ford KJ, Archila S, Davis GW. Homeostatic synaptic depression is achieved through a regulated decrease in presynaptic calcium channel abundance. Elife. 2015; 4

Gurnett CA, Felix R, Campbell KP. Extracellular interaction of the voltage–dependent Ca2+ channel alpha2delta and alpha1 subunits. J Biol Chem. 1997; 272:18508–18512. [PubMed: 9218497]

Harris N, Braiser DJ, Dickman DK, Fetter RD, Tong A, Davis GW. The Innate Immune Receptor PGRP–LC Controls Presynaptic Homeostatic Plasticity. Neuron. 2015; 88:1157–1164. [PubMed: 26687223]

Hendrich J, Van Minh AT, Heblich F, Nieto-Rostro M, Watschinger K, Striessnig J, Wratten J, Davies A, Dolphin AC. Pharmacological disruption of calcium channel trafficking by the alpha2delta ligand gabapentin. Proc Natl Acad Sci U S A. 2008; 105:3628–3633. [PubMed: 18299583]

Hoppa MB, Gouzer G, Armbruster M, Ryan TA. Control and plasticity of the presynaptic action potential waveform at small CNS nerve terminals. Neuron. 2014; 84:778–789. [PubMed: 25447742]

Hoppa MB, Lana B, Margas W, Dolphin AC, Ryan TA. alpha2delta expression sets presynaptic calcium channel abundance and release probability. Nature. 2012; 486:122–125. [PubMed: 22678293]

Kittel RJ, Wichmann C, Rasse TM, Fouquet W, Schmidt M, Schmid A, Wagh DA, Pawlu C, Kellner RR, Willig KI, et al. Bruchpilot promotes active zone assembly, Ca2+ channel clustering, and vesicle release. Science. 2006; 312:1051–1054. [PubMed: 16614170]

Kralj JM, Douglass AD, Hochbaum DR, Maclaurin D, Cohen AE. Optical recording of action potentials in mammalian neurons using a microbial rhodopsin. Nat Methods. 2012; 9:90–95.

Kurshan PT, Oztan A, Schwarz TL. Presynaptic alpha2delta-3 is required for synaptic morphogenesis independent of its Ca2+-channel functions. Nat Neurosci. 2009; 12:1415–1423. [PubMed: 19820706]

Ly CV, Yao CK, Verstreken P, Ohyama T, Bellen HJ. straightjacket is required for the synaptic stabilization of cacophony, a voltage–gated calcium channel alpha1 subunit. J Cell Biol. 2008; 181:157–170. [PubMed: 18391075]

Mahoney RE, Rawson JM, Eaton BA. An age-dependent change in the set point of synaptic homeostasis. J Neurosci. 2014; 34:2111–2119. [PubMed: 24501352]

Muller M, Davis GW. Transsynaptic control of presynaptic ca(2+) influx achieves homeostatic potentiation of neurotransmitter release. Curr Biol. 2012; 22:1102–1108. [PubMed: 22633807]

Muller M, Genc O, Davis GW. RIM-binding protein links synaptic homeostasis to the stabilization and replenishment of high release probability vesicles. Neuron. 2015; 85:1056–1069. [PubMed: 25704950]

Muller M, Liu KS, Sigrist SJ, Davis GW. RIM controls homeostatic plasticity through modulation of the readily-releasable vesicle pool. J Neurosci. 2012; 32:16574–16585. [PubMed: 23175813]

Neely GG, Hess A, Costigan M, Keene AC, Goulas S, Langeslag M, Griffin RS, Belfer I, Dai F, Smith SB, et al. A genome–wide Drosophila screen for heat nociception identifies alpha2delta3 as an evolutionarily conserved pain gene. Cell. 2010; 143:628–638. [PubMed: 21074052]

Patel R, Bauer CS, Nieto-Rostro M, Margas W, Ferron L, Chaggar K, Crews K, Ramirez JD, Bennett DL, Schwartz A, et al. alpha2delta-1 gene deletion affects somatosensory neuron function and delays mechanical hypersensitivity in response to peripheral nerve damage. J Neurosci. 2013; 33:16412–16426. [PubMed: 24133248]

Petersen SA, Fetter RD, Noordermeer JN, Goodman CS, DiAntonio A. Genetic analysis of glutamate receptors in Drosophila reveals a retrograde signal regulating presynaptic transmitter release. Neuron. 1997; 19:1237–1248. [PubMed: 9427247]

Schneggenburger R, Meyer AC, Neher E. Released fraction and total size of a pool of immediately available transmitter quanta at a calyx synapse. Neuron. 1999; 23:399–409. [PubMed: 10399944]

Schneggenburger R, Neher E. Presynaptic calcium and control of vesicle fusion. Curr Opin Neurobiol. 2005; 15:266–274. [PubMed: 15919191]

Smith PD, Liesegang GW, Berger RL, Czerlinski G, Podolsky RJ. A stopped–flow investigation of calcium ion binding by ethylene glycol bis(beta-aminoethyl ether)-N,N'-tetraacetic acid. Anal Biochem. 1984; 143:188–195. [PubMed: 6442108]

Sudhof TC. The presynaptic active zone. Neuron. 2012; 75:11–25. [PubMed: 22794257]

Thanawala MS, Regehr WG. Presynaptic calcium influx controls neurotransmitter release in part by regulating the effective size of the readily releasable pool. J Neurosci. 2013; 33:4625–4633. [PubMed: 23486937]

Wang T, Hauswirth AG, Tong A, Dickman DK, Davis GW. Endostatin is a trans-synaptic signal for homeostatic synaptic plasticity. Neuron. 2014; 83:616–629. [PubMed: 25066085]

Weyhersmuller A, Hallermann S, Wagner N, Eilers J. Rapid active zone remodeling during synaptic plasticity. J Neurosci. 2011; 31:6041–6052. [PubMed: 21508229]

Younger MA, Muller M, Tong A, Pym EC, Davis GW. A Presynaptic ENaC Channel Drives Homeostatic Plasticity. Neuron. 2013

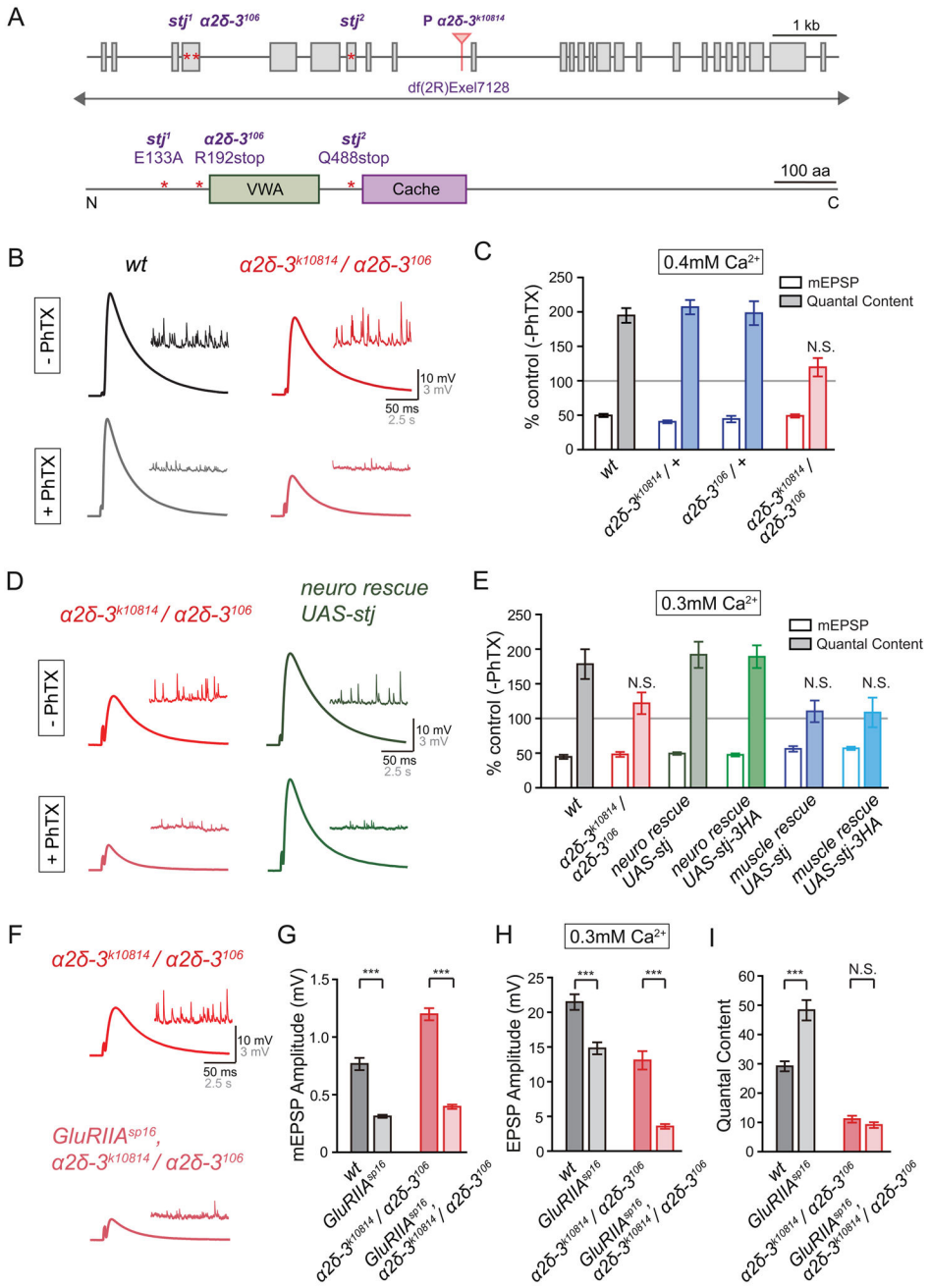

Figure 1. Mutations in *α2δ-3* Block Presynaptic Homeostatic Plasticity

(**A**) Diagram of the *Drosophila α2δ-3*gene locus (upper panel) and protein (lower panel). Coding exons are shown as grey boxes. Point mutations in the *α2δ-3* mutant alleles (*α2δ-3*^{106}, *stj*^{1}and *stj*^{2}) are indicated by red stars. The transposon insertion *α2δ-3*^{k10814} *(p[lacW]stj[k10814])* resides in an intron as indicated (red triangle). Deficiency *df*$^{(2R)Exel7128}$ uncovers the *α2δ-3* gene locus as indicated. VWA and Cache domains of the α2δ-3 protein are shown (light green and purple). See also Figure S1–S5.

(**B**) Representative traces for EPSP (scale: 10mV, 50ms) and mEPSP (scale: 3mV, 2.5s) in the absence and presence of Philanthotoxin (-PhTX, +PhTX; top and bottom, respectively)

at the wild-type (*wt*, black) and $\alpha 2\delta\text{-}3^{k10814}$ placed in *trans* to the $\alpha 2\delta\text{-}3^{106}$ mutant ($\alpha 2\delta\text{-}3^{k10814}/\alpha 2\delta\text{-}3^{106}$, red).

(**C**) mEPSP amplitudes (open bars) and presynaptic release (quantal content, filled bars) in the presence of PhTX recorded in 0.4mM extracellular calcium. Average mEPSP amplitude and quantal content are normalized to values in the absence of PhTX for each genotype. The following genotypes are presented: wild-type (*wt*, gray bars), heterozygous $\alpha 2\delta\text{-}3$mutant ($\alpha 2\delta\text{-}3^{k10814}/+$, blue bars; $\alpha 2\delta\text{-}3^{106}/+$, blue bars) and $\alpha 2\delta\text{-}3^{k10814}$ placed in *trans* to $\alpha 2\delta\text{-}3^{106}$ mutant ($\alpha 2\delta\text{-}3^{k10814}/\alpha 2\delta\text{-}3^{106}$, red bars). Mean ± SEM; N.S. not significant; Student's t-test for -PhTX and +PhTX comparisons within a single genotype.

(**D**) Representative EPSP (scale: 10mV, 50ms) and spontaneous mEPSP (scale: 3mV, 2.5s) traces in the absence and presence of PhTX (-PhTX, +PhTX; top and bottom, respectively) in $\alpha 2\delta\text{-}3^{k10814}$ placed in *trans* to $\alpha 2\delta\text{-}3^{106}$ mutant ($\alpha 2\delta\text{-}3^{k10814}/\alpha 2\delta\text{-}3^{106}$, red), and $\alpha 2\delta\text{-}3$ mutant synapses bearing an $\alpha 2\delta\text{-}3$ overexpression construct (*UAS-stj*) driven by $elav^{C155}$-*Gal4* (*neuro rescue UAS-stj*, green).

(**E**) mEPSP amplitude (open bars) and presynaptic release (quantal content, filled bars) in the presence of PhTX. The following genotypes are presented: wild-type (*wt*, gray bars), $\alpha 2\delta\text{-}3^{k10814}$ placed in *trans* to $\alpha 2\delta\text{-}3^{106}$ mutant ($\alpha 2\delta\text{-}3^{k10814}/\alpha 2\delta\text{-}3^{106}$, red), and presynaptically (*neuro rescue UAS-stj*, dark green bars; *neuro rescue UAS-stj-3HA*, light green bars), or postsynaptically (*muscle rescue UAS-stj*, dark blue bars; *muscle rescue UAS-stj-3HA*, light blue bars) expressed non-tagged (*UAS-stj*) or triple HA tagged (*UAS-stj-3HA*) $\alpha 2\delta\text{-}3$ in the $\alpha 2\delta\text{-}3$mutant background. Statistics as presented in (C).

(**F**) Representative EPSP (scale: 10mV, 50ms) and mEPSP (scale: 3mV, 2.5s) traces recorded at the $\alpha 2\delta\text{-}3^{k10814}$ placed in *trans* to $\alpha 2\delta\text{-}3^{106}$ mutant ($\alpha 2\delta\text{-}3^{k10814}/\alpha 2\delta\text{-}3^{106}$, red) and $GluRIIA^{sp16},\alpha 2\delta\text{-}3^{k10814}/\alpha 2\delta\text{-}3^{106}$ double mutant NMJ ($GluRIIA^{sp16},\alpha 2\delta\text{-}3^{k10814}/\alpha 2\delta\text{-}3^{106}$, light red) in 0.3mM extracellular calcium.

(**G**) – (**I**) Average mEPSP amplitude (G), EPSP amplitude (H), presynaptic release (I, quantal content) recorded in 0.3mM extracellular calcium. The following genotypes are presented: wild-type (*wt*, black bars), $GluRIIA^{sp16}$ (gray bars), $\alpha 2\delta\text{-}3^{k10814}/\alpha 2\delta\text{-}3^{106}$ (red bars), and $GluRIIA^{sp16},\alpha 2\delta\text{-}3^{k10814}/\alpha 2\delta\text{-}3^{106}$ (light red bars). Mean ± SEM; ***$p < 0.001$, N.S. not significant; Student's t-test.

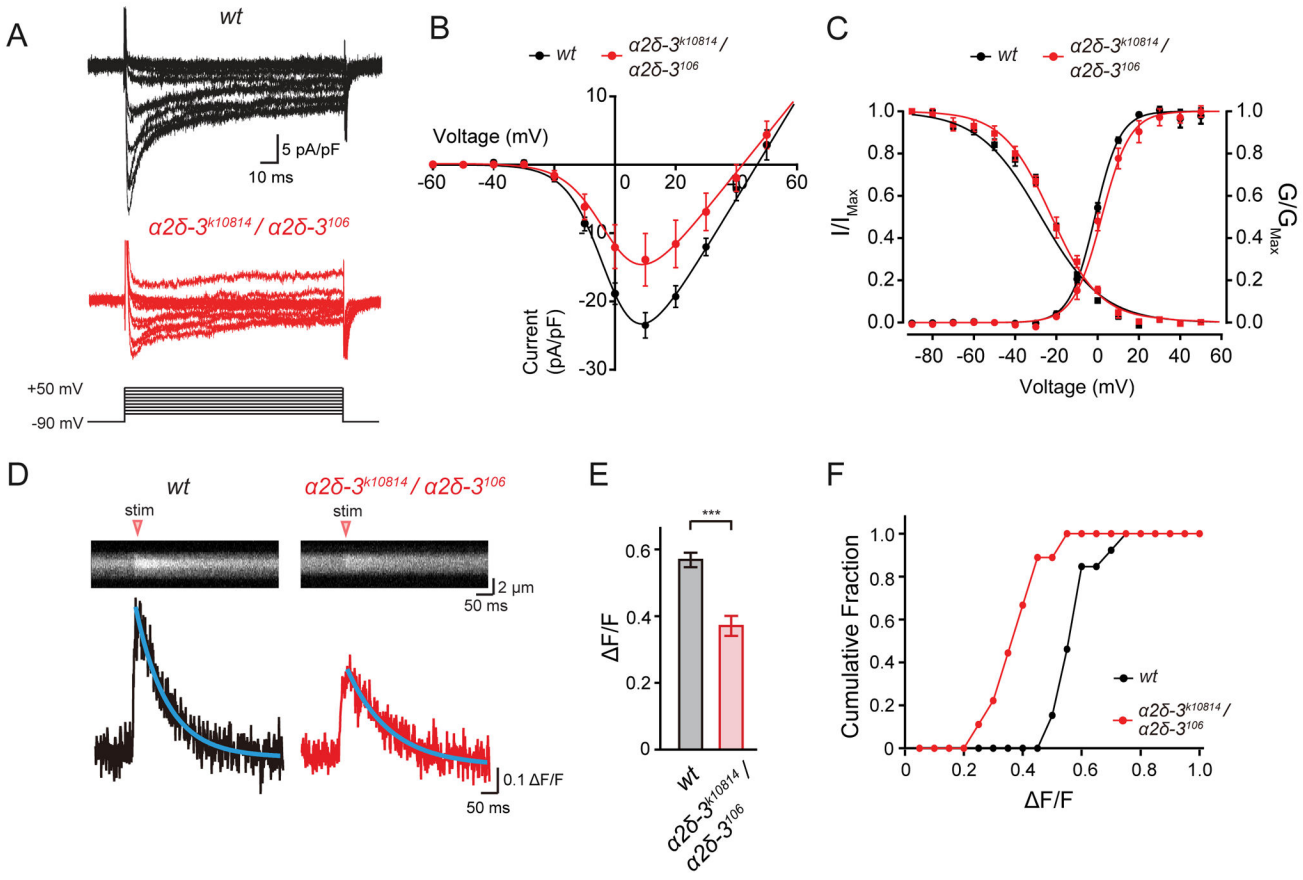

Figure 2. *α2δ-3* Mutants Have Reduced Calcium Current Density in Motoneuron Soma and Reduced Calcium Influx at Presynaptic Terminals

(**A**) Representative Ca^{2+} currents (I_{Ca}) in motoneurons elicited by 120ms voltage steps from −90 to +50mV, measured in wild-type (*wt*, black) and *α2δ-3* mutant (*α2δ-3*^{k10814}/*α2δ-3*^{106}, red); scale: 5pA/pF, 10ms.

(**B**) I–V plots of both peak I_{Ca} reveal significantly reduced I_{Ca} current density in *α2δ-3*^{k10814}/*α2δ-3*^{106} (n=11, red) compared to wild-type (n=9, black, $p < 0.001$). Currents are normalized for cell capacitance (pA/pF) and I-V plots were fit with modified Boltzmann equations. Mean ± SEM; Student's t-test.

(**C**) Calcium channel activation (G/G_{max}) and steady-state inactivation (I/I_{max}) curves in wild-type (n=9, black) and *α2δ-3*^{k10814}/*α2δ-3*^{106} (n=11, red). I/I_{max} and G/G_{max} curves were fit with modified Boltzmann equations. Activation $V_{1/2}$ or steady-state inactivation $V_{1/2}$ are not different between genotypes; Student's t-test.

(**D**) Representative traces of single AP-evoked, spatially averaged calcium transients measured by line scans of in wild-type (*wt*, black) and the *α2δ-3* mutant (*α2δ-3*^{k10814}/*α2δ-3*^{106}, red) animal NMJs. Wild-type and *α2δ-3* mutant data are fit with a single exponential decay (blue lines).

(**E**) Average calcium transient peak amplitudes (F/F) in wild-type (*wt*, n=13, black bar) and *α2δ-3* mutant (*α2δ-3*^{k10814}/ *α2δ-3*^{106}, n=9, red bar). Mean ± SEM; ***$p < 0.001$; Student's t-test.

(**F**) Cumulative frequencies of F/F peak amplitudes in wild-type (*wt*, black line) and *α2δ-3* mutant (*α2δ-3*^{k10814}/*α2δ-3*^{106}, red line).

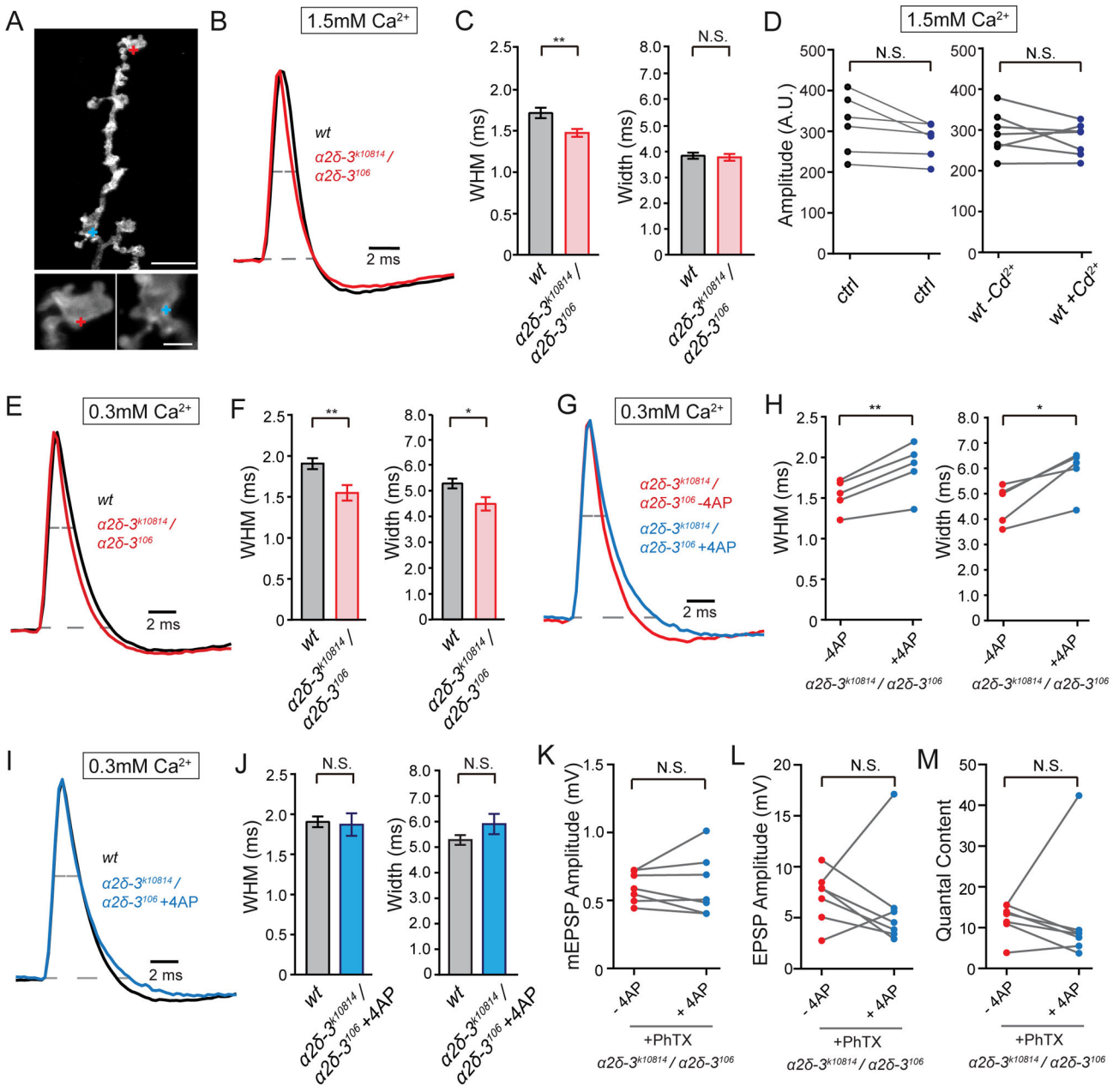

Figure 3. Presynaptic Action Potential Waveforms Imaged with Archaerhodopsin

(**A**) Representative fluorescence images for the *Drosophila* NMJ expressing Arch-GFP. Red and blue crosses indicate the location of point scans. See also Figure S6.

(**B**) Average traces of single action potentials in wild-type (*wt*, black) and the *α2δ-3* mutant ($\alpha2\delta\text{-}3^{k10814}/\alpha2\delta\text{-}3^{106}$, red) in 1.5mM extracellular calcium. Voltage traces for wild-type and *α2δ-3* mutant are normalized to peak amplitude (see methods).

(**C**) Average width half max (WHM) and width for wild-type (*wt*, n=13, black bars) and *α2δ-3* mutant synapses ($\alpha2\delta\text{-}3^{k10814}/\alpha2\delta\text{-}3^{106}$, n=13, red bars) in 1.5mM extracellular calcium. Mean ± SEM; **p < 0.01, N.S. not significant; Student's t-test.

(**D**) Average amplitude of action potentials before and after cadmium treatment in wild-type (1.5mM extracellular calcium). Action potentials amplitudes for synaptic boutons before (average=317.1±29.7 A.U.) and after control saline treatment (average=278.2±17.9 A.U., n=6), and action potential amplitudes before (average=292.9±19.9 A.U.) and after (average = 277.2±15.2 A.U., n=7) cadmium (3μM) treatment. A.U.=arbitrary units; N.S. not significant; Student's t-test, paired.

(**E**) Action potentials measured by spot scans in wild-type (*wt*, black) and the *α2δ-3* mutant (*α2δ-3*^{k10814}/*α2δ-3*^{106}, red) (0.3mM extracellular calcium) normalized as in (B).

(**F**) Average width half max (WHM) and width for wild-type (*wt*, n=15, black bars) and *α2δ-3* (*α2δ-3*^{k10814}/*α2δ-3*^{106}, n=9, red bars) at 0.3mM extracellular calcium. Mean ± SEM; *p < 0.05, **p < 0.01; Student's t-test.

(**G**) Action potentials measured by spot scans in *α2δ-3* before (*α2δ-3*^{k10814}/*α2δ-3*^{106}, -4AP, red) and after 100μM 4AP treatment (*α2δ-3*^{k10814}/*α2δ-3*^{106}, +4AP, blue) in 0.3mM extracellular calcium. Traces normalized as in (B).

(**H**) Average width half max (WHM) and width for *α2δ-3* mutant synapses before (*α2δ-3*^{k10814}/*α2δ-3*^{106}, -4AP, mean WHM=1.53±0.09 ms, mean Width=4.60±0.35 ms, n=5, red) and after 100μM 4-AP treatment (*α2δ-3*^{k10814}/*α2δ-3*^{106}, +4AP, mean WHM=1.87±0.14 ms, mean Width=5.91±0.40 ms, n=5, blue) in 0.3mM extracellular calcium. Mean ± SEM; *p < 0.05, **p < 0.01; Student's t-test, paired.

(**I**) Action potentials measured by spot scans in wild-type without 4AP treatment (*wt*, -4AP, black) and *α2δ-3* in the presence of 4AP (*α2δ-3*^{k10814}/*α2δ-3*^{106}, +4AP, blue) in 0.3mM extracellular calcium. Traces normalized as in (B)

(**J**) Average width half max (WHM) and width for wild-type NMJ without 4AP treatment (*wt*, -4AP, n=15, black bars) and *α2δ-3* mutant animal NMJ with 4AP treatment (*α2δ-3*^{k10814}/*α2δ-3*^{106}, +4AP, n=5, blue bars) in 0.3mM extracellular calcium. Mean ± SEM; N.S. not significant; Student's t-test.

(**K**) – (**M**) mEPSP amplitude (K), EPSP amplitude (L) and synaptic transmission (M, quantal contents) in PhTX incubated *α2δ-3* mutant animal NMJ before (*α2δ-3*^{k10814}/*α2δ-3*^{106}, -4AP, red, n=7) and after (*α2δ-3*^{k10814}/*α2δ-3*^{106}, +4AP, blue, n=7) 100μM 4AP treatment. Mean ± SEM; N.S. not significant; Student's t-test, paired.

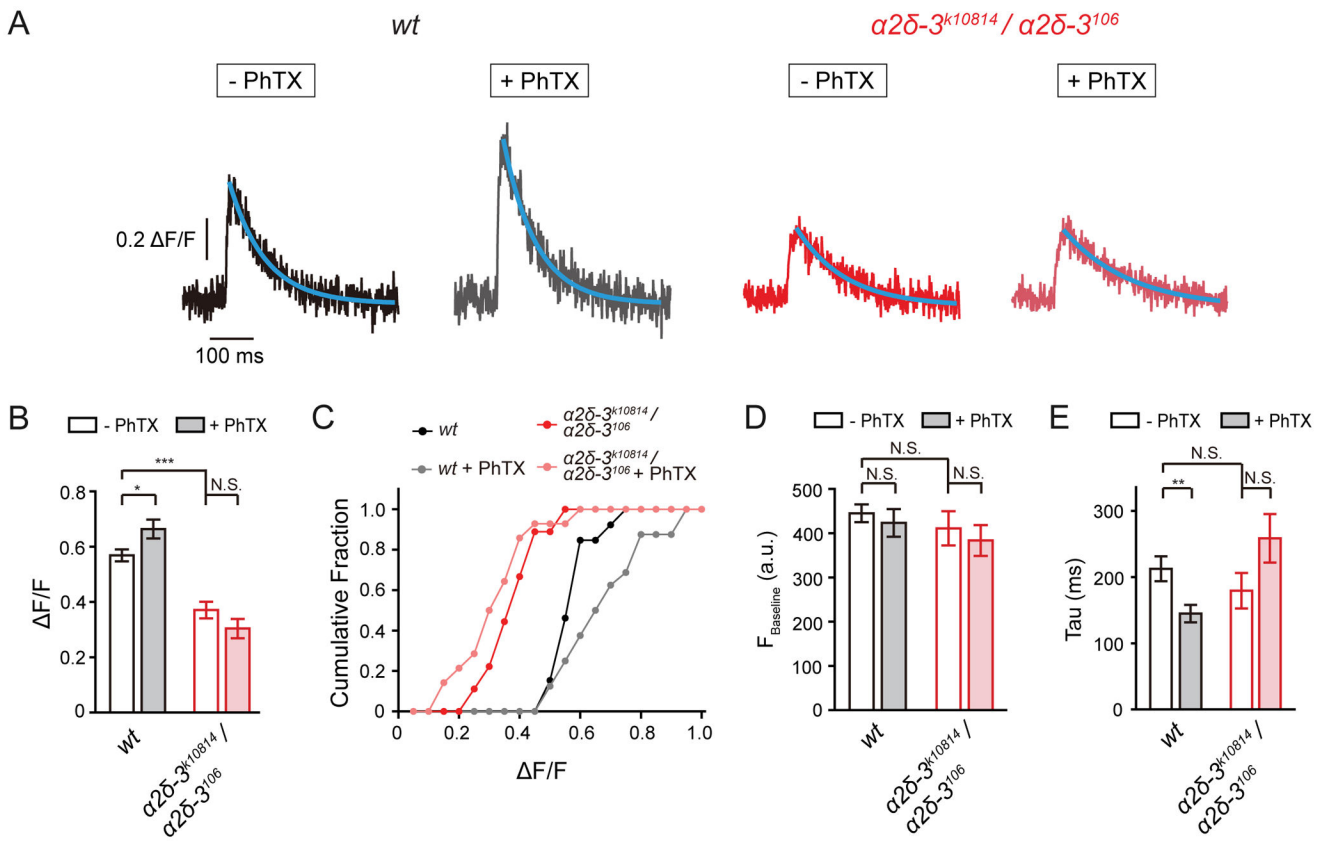

Figure 4. Impaired Homeostatic Potentiation of Presynaptic Calcium Influx in *α2δ-3* Mutants

(**A**) Representative traces of single AP-evoked, spatially averaged calcium transients measured by line scans in the absence or presence of PhTX (-PhTX, +PhTX) in wild-type (*wt*, black) and the *α2δ-3* mutant (*α2δ-3*^{k10814}/*α2δ-3*^{106}, red). Wild-type and *α2δ-3* mutant data are fit with single exponential decay (blue lines).

(**B**) Average calcium transient peak amplitudes (F/F) in the absence (-PhTX, open bars) or presence of PhTX (+PhTX, filled bars) for wild-type (*wt*, -PhTX, n=13, black bars; wt, +PhTX, n=16, gray bars) and *α2δ-3* mutant (*α2δ-3*^{k10814}/*α2δ-3*^{106}, -PhTX, n=9, red bars; *α2δ-3*^{k10814}/*α2δ- 3*^{106}, +PhTX, n=14, light red bars). Mean ± SEM; *p < 0.05, ***p < 0.001, N.S. not significant; Student's t-test.

(**C**) Cumulative frequencies of F/F peak amplitudes in wild-type (*wt*, -PhTX, black line; *wt*, +PhTX, gray lines) and *α2δ-3* mutant boutons (*α2δ-3*^{k10814}/*α2δ-3*^{106}, -PhTX, red line; *α2δ-3*^{k10814}/*α2δ-3*^{106}, +PhTX, light red line).

(**D**) – (**E**) Average baseline fluorescence ($F_{baseline}$, D) and average decay time constant (Tau, E) in the absence (-PhTX, open bars) or presence of PhTX (+PhTX, filled bars) for wild-type (*wt*, black bars) and *α2δ-3* mutant boutons (*α2δ-3*^{k10814}/*α2δ-3*^{106}, red bars). Mean ± SEM; **p < 0.01, N.S. not significant; Student's t-test.

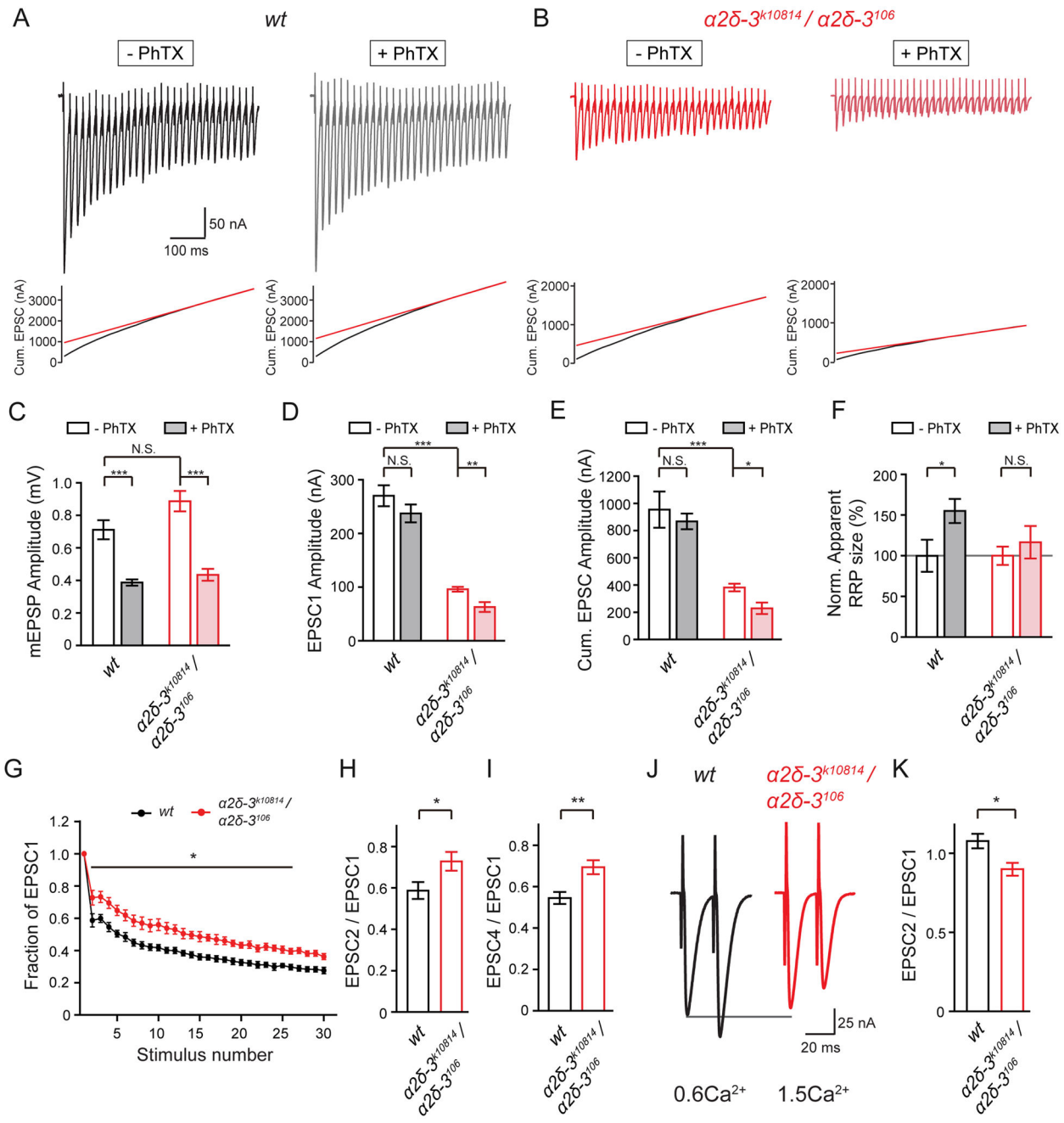

Figure 5. *α2δ-3* Mutants Lack Homeostatic Modulation of RRP and Exhibit Abnormal Short-term Plasticity

(**A**) – (**B**) Representative EPSC trains (scale: 50nA, 100ms, upper panels) in response to 60Hz (30 stimuli) stimulation in 1.5mM extracellular calcium at the wild-type (*wt*, black, A) and the *α2δ-3* mutant (*α2δ-3*^{k10814}/*α2δ-3*^{106}, red, B) in the absence or presence of PhTX (-PhTX, +PhTX). Cumulative EPSC (black lines, lower panels) for each genotype and the line fit to the cumulative EPSC data that was back-extrapolated to time 0 (red lines) are presented for each condition.

(**C**) – (**E**) Average mEPSP amplitude (C), average first EPSC amplitude during the train (EPSC1, D), and cumulative EPSC amplitude (cum. EPSC, E) in wild-type (*wt*, black bars) and *α2δ-3* mutant (*α2δ-3*^{k10814}/*α2δ-3*^{106}, red bars) in the absence (-PhTX, open bars) or presence of PhTX (+PhTX, filled bars). Mean ± SEM; *p < 0.05, **p < 0.01, ***p < 0.001, N.S. not significant; Student's t-test.

(**F**) Quantification of estimated RRP (cum. EPSC / mEPSP) in wild-type (*wt*, black bars) and *α2δ-3* mutant (*α2δ-3*^{k10814}/*α2δ-3*^{106}, red bars) in the absence (-PhTX, open bars) or presence of PhTX (+PhTX, filled bars). Average estimated RRP is normalized to baseline values for the wild-type and *α2δ-3* mutants. Mean ± SEM; Statistics as in (C).

(**G**) Average amplitude of EPSCs during 60Hz train stimulation at the wild-type (*wt*, black) and the *α2δ-3* mutant (*α2δ-3*^{k10814}/*α2δ-3*^{106}, red) NMJ in the absence of PhTX. EPSC amplitude during the train is normalized to the amplitude of the first EPSC for each genotype. Mean ± SEM; *p < 0.05 two-way repeated measures ANOVA, Bonferroni's test.

(**H**) Paired-pulse ratio (the ratio between the amplitudes of the second and first EPSCs, EPSC2/EPSC1) at 60Hz stimulation in wild-type (*wt*, n=8, black bar) and *α2δ-3* mutant (*α2δ-3*^{k10814}/*α2δ-3*^{106}, n=8, red bar). Mean ± SEM; *p < 0.05, **p < 0.01; Student's t-test.

(**I**) Paired-pulse ratio (the ratio between the amplitudes of the forth and first EPSCs, EPSC4/EPSC1) at 60Hz stimulation in wild-type (*wt*, black bar) and *α2δ-3* (*α2δ-3*^{k10814}/*α2δ-3*^{106}, red bar). Mean ± SEM; Statistics as in (H).

(**J**) Representative paired-pulse EPSC traces (scale: 25nA, 20ms) in response to 50Hz stimulation in 0.6mM extracellular calcium in wild-type (*wt*, black) and in 1.5mM extracellular calcium in *α2δ-3* mutant (*α2δ-3*^{k10814}/*α2δ-3*^{106}, red).

(**K**) Paired-pulse ratio (the ratio between the amplitudes of the second and first EPSCs, EPSC2/EPSC1) at 50Hz stimulation in wild-type (*wt*, n=7, black bar) in 0.6mM extracellular calcium, and *α2δ-3* mutant (*α2δ-3*^{k10814}/*α2δ-3*^{106}, n=9, red bar) in 1.5mM extracellular calcium. Mean ± SEM; *p < 0.05; Student's t-test.

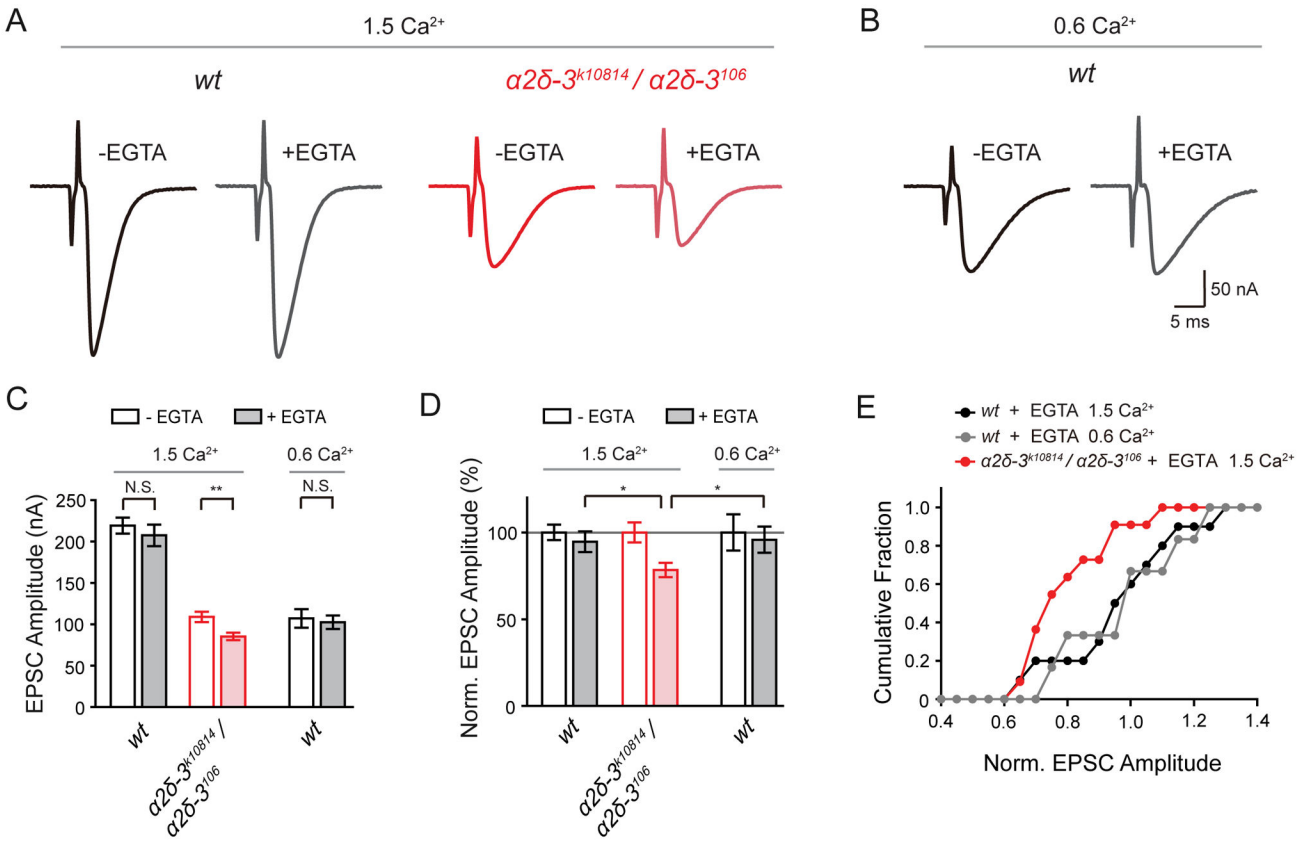

Figure 6. *α2δ-3* Mutants Have Increased EGTA Sensitivity

(**A**) Representative EPSC traces (scale: 50nA, 5ms) in wild-type (*wt*, black) and *α2δ-3* mutant (*α2δ-3*^{k10814}/*α2δ-3*^{106}, red) at 1.5mM extracellular calcium in the absence (-EGTA) or presence of EGTA (+EGTA).

(**B**) Representative EPSC traces at wild-type (*wt*, black) in 0.6mM extracellular calcium in the absence (-EGTA) or presence of EGTA (+EGTA).

(**C**) Average EPSC amplitude for wild-type (*wt*, black bars, left), *α2δ-3* mutant (*α2δ-3*^{k10814}/*α2δ-3*^{106}, red bar, left) in 1.5mM extracellular calcium, and wild-type (*wt*, black bars, right) in 0.6mM extracellular calcium in the absence (-EGTA, open bars) and presence of EGTA (+EGTA, filled bars). Mean ± SEM; **p < 0.01, N.S. not significant; Student's t-test.

(**D**) Data as in (C) for normalized EPSC amplitudes. Mean ± SEM; *p < 0.05; Student's t-test.

(**E**) Cumulative frequency for wild-type (*wt*, black), *α2δ-3* mutant (*α2δ-3*^{k10814}/*α2δ-3*^{106}, red) in 1.5mM extracellular calcium, and wild-type (*wt*, gray) in 0.6mM extracellular calcium in the presence of EGTA. EPSC amplitude in the presence of EGTA is normalized to the EPSC amplitude in the absence of EGTA for each genotype.

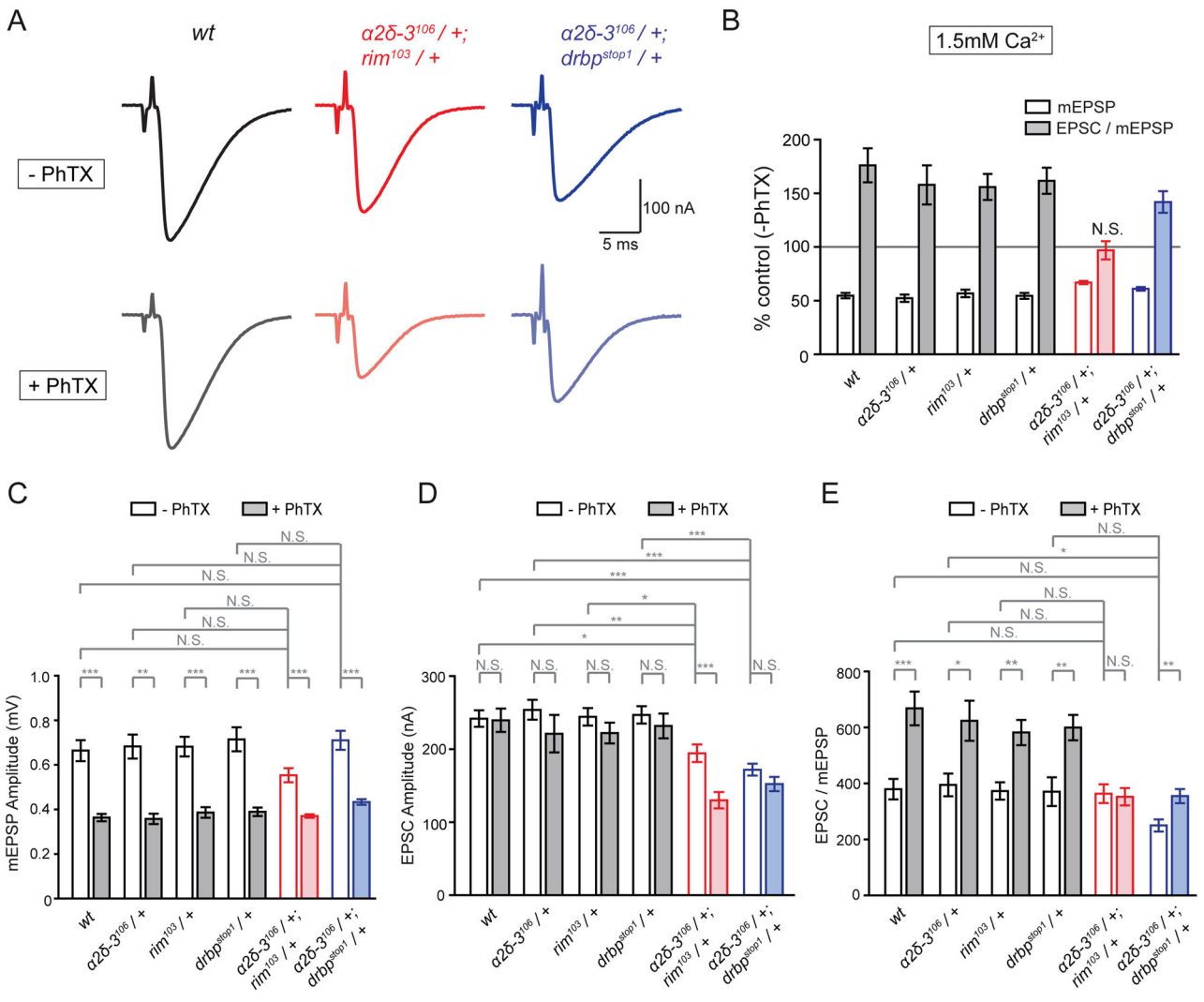

Figure 7. *α2δ-3* Interacts with *rim* during Synaptic Homeostasis

(**A**) Representative traces for EPSC (scale: 100nA, 5ms) traces in the absence and presence of PhTX (-PhTX, +PhTX; top and bottom respectively) in wild-type (*wt*, black) and heterozygous $\alpha2\delta\text{-}3^{106}$ mutant placed *in trans* with rim^{103} ($\alpha2\delta\text{-}3^{106}/+;rim^{103}/+$, red) and $drbp^{stop1}$ ($\alpha2\delta\text{-}3^{106}/+;drbp^{stop1}/+$, blue) mutants. See also Figure S7.

(**B**) mEPSP amplitude (open bars) and presynaptic release (EPSC/mEPSP, filled bars) in the presence of PhTX. Average mEPSP amplitude and EPSC/mEPSP are normalized to values in the absence of PhTX for each genotype. The following genotypes are presented: wild-type (*wt*, gray bars), heterozygous $\alpha2\delta\text{-}3^{106}$ mutant ($\alpha2\delta\text{-}3^{106}/+$, gray bars), heterozygous rim^{103} mutant ($rim^{103}/+$, gray bars), heterozygous $drbp^{stop1}$ mutant ($drbp^{stop1}/+$, gray bars), heterozygous mutants of $\alpha2\delta\text{-}3^{106}$and rim^{103}placed in *trans* ($\alpha2\delta\text{-}3^{106}/+;rim^{103}/+$, red bars), and heterozygous mutants of $\alpha2\delta\text{-}3^{106}$ and $drbp^{stop1}$ placed in *trans* ($\alpha2\delta\text{-}3^{106}/+;drbp^{stop1}/+$, blue bars). Mean ± SEM; N.S. not significant; Student's t-test for -PhTX and +PhTX comparisons.

(**C**) – (**E**) Quantification of synaptic transmission for genotypes represented in (B) in the absence (-PhTX) or presence of (+PhTX) PhTX. Average mEPSP amplitude (C), EPSC

amplitude (D) and presynaptic release (EPSC/mEPSP, E) in the absence or presence of PhTX. Genotypes as in (B). Mean ± SEM; *p < 0.05, **p < 0.01, ***p < 0.001, N.S. not significant; Student's t-test for -PhTX and +PhTX comparisons, one-way ANOVA and Bonferroni's test for basal transmission across genotypes.